Thermodynamic Calculations in the System CH_4-H_2O and Methane Hydrate Phase Equilibria

Susan Circone, Stephen H. Kirby, and Laura A. Stern*

U.S. Geological Survey, 345 Middlefield Rd. MS 977, Menlo Park, California 94025

Received: September 23, 2005; In Final Form: January 20, 2006

Using the Gibbs function of reaction, equilibrium pressure, temperature conditions for the formation of methane clathrate hydrate have been calculated from the thermodynamic properties of phases in the system CH_4−H_2O. The thermodynamic model accurately reproduces the published phase-equilibria data to within ±2 K of the observed equilibrium boundaries in the range 0.08−117 MPa and 190−307 K. The model also provides an estimate of the third-law entropy of methane hydrate at 273.15 K, 0.1 MPa of 56.2 J mol^{-1} K^{-1} for 1/*n* CH_4·H_2O, where *n* is the hydrate number. Agreement between the calculated and published phase-equilibria data is optimized when the hydrate composition is fixed and independent of the pressure and temperature for the conditions modeled.

Introduction

Structure I methane hydrate is a crystalline compound comprised of a hydrogen-bonded H_2O lattice with small (pentagonal dodecahedral) and large (tetrakaidecahedral) cages that may each contain one molecule of CH_4. The structure I unit cell consists of 46 H_2O molecules and eight cages, in a ratio of one small to three large. Methane hydrate forms via one of these reactions:

$$CH_4\,(g) + nH_2O\,(s) = CH_4{\cdot}nH_2O\,(s) \qquad (1a)$$

or

$$CH_4\,(g) + nH_2O\,(l) = CH_4{\cdot}nH_2O\,(s) \qquad (1b)$$

depending on whether pressure and temperature (*P* and *T*) conditions are below or above the H_2O melting point. If all cages are filled with methane, the composition is $CH_4{\cdot}5.75H_2O$, where 5.75 is referred to as the hydrate number, *n*. However, gas clathrate hydrates are nonstoichiometric with some cages vacant (i.e., *n* is greater than 5.75 for structure I hydrates, including methane).

Phase-equilibria data for methane hydrate are available from several studies,[1] spanning conditions from 148.8 K and 0.0053 MPa to 326.8 K and 1000 MPa. Historically, the pressure and temperature conditions of hydrate equilibrium boundaries, like those described by reaction 1, have been modeled using a statistical thermodynamic approach first developed by van der Waals and Platteeuw.[2] With an accuracy dependent in large part on the value for the difference in chemical potential between water and the hypothetical empty hydrate lattice, these models can reproduce the three-phase boundaries of gas−ice−hydrate and gas−water−hydrate for a number of hydrate-forming gases and mixtures. The hydrate number and distribution of gases between small and large cages can also be calculated.

In this study, we have taken a classical thermodynamic approach to model reaction 1, in which model parameters are bulk thermodynamic properties of materials that are measured directly through experiment. We start with the equation

$$\Delta G(T,P) = \Delta H^{\ominus}(T) - T\Delta S^{\ominus}(T) + \Delta\int_{P^{\ominus}}^{P} V(T,P)\,dP \qquad (2)$$

and use standard-state conditions ($T^{\ominus}$, $P^{\ominus}$) of 273.15 K, 0.1 MPa for all phases. At equilibrium, the $\Delta G(T,P)$ of the product minus reactants for reaction 1 is equal to 0 J mol^{-1}. The enthalpy of reaction at temperature, $\Delta H^{\ominus}(T)$, is defined as

$$\Delta H^{\ominus}(T) = \Delta H^{\ominus}(T^{\ominus}) + \int_{T^{\ominus}}^{T} \Delta C_p\,dT \qquad (3)$$

The entropy of reaction at temperature, $\Delta S^{\ominus}(T)$, is defined as

$$\Delta S^{\ominus}(T) = \Delta S^{\ominus}(T^{\ominus}) + \int_{T^{\ominus}}^{T} \frac{\Delta C_p}{T}\,dT \qquad (4)$$

The molar volumes of the liquid and solid phases were fit to the following equations:[3]

$$V(T,P) = V^{\ominus}(T^{\ominus})\,\upsilon(T)\,\upsilon(P) \qquad (5)$$

where $\upsilon(T)$ describes the thermal expansion of the phase with reference to the standard state as

$$\upsilon(T) = 1 + \int_{T^{\ominus}}^{T} (\alpha_0 + \alpha_1 T + \alpha_2 T^2)\,dT \qquad (6)$$

and $\upsilon(P)$ describes the compressibility of the phase with reference to the standard state using the isothermal bulk modulus K_T and its pressure derivative K'

$$\upsilon(P) = \left(1 + \frac{K'P}{K_T}\right)^{-\frac{1}{K'}} \qquad (7)$$

Thus, eq 7 can be integrated over the pressure range of interest to calculate the pressure dependence of the Gibbs free energy

* To whom correspondence should be addressed. E-mail: lstern@usgs.gov. Phone: 650-329-4811. Fax: 650-329-5163.

10.1021/jp055422f CCC: $33.50
Published on Web 04/04/2006

of reaction for the liquid and solid phases. The effect of pressure on the Gibbs free energy of methane gas is

$$\int_{P^\ominus}^{P} V(T,P)\,dP = RT\ln(f_P/f_{P^\ominus}) \quad (8)$$

where f_P is the methane fugacity at T and P.

Using this classical thermodynamic approach, the Gibbs free energy of the reaction can be calculated for pressure, temperature conditions both on or away from the equilibrium boundary, the latter being a factor in kinetic studies of hydrate formation and dissociation. However, it has not been used previously to model the CH_4-H_2O system due to the limited availability of thermodynamic data for methane hydrate. In recent years, measurements on well-characterized samples have better constrained some properties of methane hydrate. As reviewed in a recent study,[4] direct measurement of hydrate composition has yielded hydrate numbers in the range of 5.8−6.3 at pressures of 2−13 MPa near the equilibrium boundary.[4−6] An average composition of $CH_4 \cdot 5.99 \pm 0.07\ H_2O$ was measured at pressures of 1.9−9.7 MPa, after annealing at conditions just within the equilibrium boundary.[4] Within experimental uncertainty, n does not depend on the pressure−temperature conditions. Using Raman spectroscopy, the distribution of methane between small and large cages has also been determined over a wider pressure range (3.5−72.5 MPa).[7] Yet some uncertainties remain. The third-law entropy for methane hydrate has not been measured, the thermal expansion of methane hydrate has not been determined at higher temperatures, nor has the hydrate composition been measured over the wide P and T range encompassed in the phase equilibria experiments.

We have undertaken a series of calculations using eqs 2−8 and the available thermodynamic data. We compare the results to the experimentally determined phase equilibria for reaction 1 over a wide pressure and temperature range, namely 148.8−320 K and 0.0053−405 MPa. Based on results from these calculations, some useful constraints can be placed on the uncertainties discussed above. The results are also compared to those obtained using a statistical thermodynamic model (CSMHYD) developed by Sloan and others at the Colorado School of Mines.[1]

It is important to note that results from careful phase equilibria experiments best constrain the location of reaction boundaries. A thermodynamic model, especially a classical one based on independently measured parameters, will never be as accurate as an empirical fit to existing phase equilibria data. Instead, this model's strength lies in two areas: (1) its ability to calculate, with some certainty, the thermodynamic properties and relative Gibbs free energies over the range of P and T conditions covered by the thermodynamic data, including but not limited to the equilibrium boundaries, and (2) its use of model parameters that are directly, if not always easily, measurable physical properties of the phases involved.

Methodology

The thermodynamic data used to calculate the Gibbs free energy of reaction 1 with eqs 2−8 were gathered from a variety of sources. Thermodynamic data for methane hydrate are reported on a per mole of H_2O basis (i.e., $1/n\ CH_4 \cdot H_2O$), since the amount of water directly determines the molar volume of the hydrate. These data are then multiplied by the selected hydrate number (see below). The enthalpy of reaction at 273.15 K for reaction 1b has been determined by calorimetry to be -9032 ± 47 J mol^{-1} for methane hydrate with composition $1/6\ CH_4 \cdot H_2O$ formed from CH_4(g) and H_2O (l).[6] Heat capacity data were fit to a polynomial:

$$C_p = a + bT + cT^2 + dT^3 \quad (9)$$

Table 1 summarizes the heat capacity parameters and standard-state entropies $S^\ominus(T^\ominus)$ used for CH_4, H_2O (l and s), and $1/n\ CH_4 \cdot H_2O$. Thus, the enthalpy of reaction $\Delta H^\ominus(T)$ for reaction 1b is calculated using eq 3 and -9032 J mol^{-1} for $\Delta H^\ominus(T^\ominus)$, whereas that for reaction 1a is calculated using $\Delta H^\ominus(T^\ominus) = -3022$ J mol^{-1}, the difference being equivalent to the enthalpy of freezing one mole of the reactant H_2O. The negative of eq 3 is equivalent to calculating the enthalpy of dissociation of methane hydrate as a function of temperature. The entropy of reaction $\Delta S^\ominus(T)$ is calculated from the entropy difference of product and reactants using eq 4. As noted in the Introduction, the third-law entropy for methane hydrate has not yet been determined by low-temperature calorimetric methods. We have allowed this value to vary to minimize the Gibbs free energy of reaction 1. This is discussed in further detail below.

In Table 2, we summarize the thermal expansion and compressibility parameters used for the equation of state (eqs 5−7). The molar volume of methane hydrate was extrapolated from powder neutron and X-ray diffraction data collected between 4 and 170 K at 0.1 MPa.[15] An additional constraint can be placed on the molar volume at 271 K using the isothermal compressibility measurements of Klapproth et al.[16] between 3.4 and 100 MPa (Figure 1). The molar volume data were then recast in terms of eq 6 to obtain the parameters $\alpha_{0,1,2}$ for the thermal expansion of methane hydrate with respect to the extrapolated standard state at 273.15 K (Table 2). We have used results from the wave speed measurements of Helgerud et al.[23] for the methane hydrate bulk modulus. At 271 K and 60 MPa, a bulk modulus of 9000 MPa is calculated using their equation: $K(T,P) = 8762 - 9.71T + 3.64P$, with T in °C and P in MPa. This is comparable to the isothermal bulk modulus (9110 MPa) obtained by Klapproth et al.[16] at those conditions.

Next, the hydrate number and distribution of methane in small and large cages in the hydrate structure must be considered. Direct measurement of methane hydrate composition has yielded an average value of 5.99 ± 0.07 along the equilibrium boundary at 2 to 10 MPa.[4] Both nuclear magnetic resonance and Raman spectroscopy have provided information on the relative distribution of methane between small and large cages, based on the relative peak areas attributed to methane in the two cages. Using ^{13}C NMR spectroscopy, an occupancy ratio for small to large cages of 0.916 was determined for a methane hydrate sample synthesized at 233.15 K and then annealed at 260.15 K (P conditions for synthesis and anneal were not provided).[24] Recently, the distribution of methane between small and large cages was determined as a function of pressure by Raman spectroscopy.[7] Measurements were made between 3.5 and 72.5 MPa at temperatures within 1 K of the equilibrium boundary (Figure 2a). The small to large cage occupancy ratio (x_S/x_L) increases with increasing pressure over the measured pressure interval. We fit the pressure dependence of the ratio to an empirical equation

$$x_S/x_L = 0.84533 + 0.086671 \log_{10}(P) \quad (10)$$

These experimental results and other possible methane distributions are applied to the model (see below). As previously mentioned, structure I hydrate unit cell contains 2 small and 6

TABLE 1: Third-Law Entropies at 273.15 K, 0.1 MPa (in J mol^{-1} K^{-1}) and Eq 9 Parameters for the Heat Capacities of Phases in the System CH_4-H_2O

phase	T range (K)	a	b	c	d	$S^{\ominus}(T^{\ominus})$
CH_4 (g)[a]	120−600	$+4.3297 \times 10$	-1.0737×10^{-1}	$+3.4623 \times 10^{-4}$	-2.3633×10^{-7}	183.17
H_2O (s)[b]	15−273.15	−2.3134	$+2.3339 \times 10^{-1}$	-6.5559×10^{-4}	$+1.2497 \times 10^{-6}$	41.34
H_2O (l)[b]	273.15−373.15	$+2.2851 \times 10^{2}$	−1.3423	$+3.8805 \times 10^{-3}$	-3.6963×10^{-6}	63.34
$1/n$ $CH_4 \cdot H_2O$ (s)[c]	85−270	+1.1569	2.4113×10^{-1}	-5.9763×10^{-4}	1.0284×10^{-6}	~56.2

[a] Heat capacity fit to tabulated values in Table II.17 of Sychev et al.[8] over T range indicated. Standard-state entropy calculated from tabulated value of 186.26 J mol^{-1} K^{-1} at 298.15 K[9] and the heat capacity (equation 4, using reference T of 298.15 and a new T of 273.15 K). Value is consistent with tabulated data in Sychev et al.[8] [b] CODATA Key Values for Thermodynamics:[10] ΔS of the phase transition H_2O (s) = H_2O (l) is 22.00 J mol^{-1} K^{-1} at 273.15 K, and ΔH of the phase transition is 6009 J mol^{-1} at 273.15 K. [c] Heat capacity eq 9 fit to tabulated values in Table 3 of Handa;[6] extrapolation of +50 K is necessary to cover range of modeled phase-equilibria data. The standard-state entropy has not yet been measured but is estimated in this study (see text).

TABLE 2: Standard-State Molar Volumes and Other Parameters Used in Calculating the Equation of State of H_2O (s,l) and $1/n$ $CH_4 \cdot H_2O$[h]

	H_2O (s)	H_2O (l)	$1/n$ $CH_4 \cdot H_2O$
$V^{\ominus}(T^{\ominus})$ (cm^3 mol^{-1})	19.652[a]	18.018[b]	22.377[c]
α_0 (K^{-1})	-5.668×10^{-5}	-1.626×10^{-2}	-6.135×10^{-7}
α_1 (K^{-2})	9.229×10^{-7}	1.005×10^{-4}	1.236×10^{-6}
α_2 (K^{-3})	-3.209×10^{-10}	-1.510×10^{-7}	-2.126×10^{-9}
$K_T^{\ominus}$(MPa)	8726.4[d]	1944.3[e]	8762[f]
dK/dT (MPa K^{-1})[g]	−8.95	15.031 −0.15707	−9.71
K'	4.66	6.5	3.64

[a] Molar volume[11] and parameters from fit to volumetric thermal expansion data over the T range of 70 to 273.15 K.[11−12] [b] Molar volume from Table 94 of Dorsey.[13] For volumetric thermal expansion parameters, we fit the 0.1 MPa data from Dorsey[13] (T range of 260 to 303 K) and the tabulated density data in The Handbook of Physical Constants[14] (273.15 to 333.15 K). [c] Molar volume extrapolated from low-temperature diffraction data.[15,16] See Figure 1 and text for further discussion of methane hydrate thermal expansion fit. [d] $K_T^{\ominus}$ and dK/dT from several studies between 50 and 258 K.[17−20] K' measured at 237.5 K over P range of 0.1 to 280 MPa.[21] [e] $K_T^{\ominus}$, K_T, and K' obtained by fitting the volumetric data in Table 95 of Dorsey[13] and the tabulated data in Burnham et al.[22] (data range: 273.15 to 333.15 K at 20 K intervals, 0.1 to 500 MPa). Data were fit to eq 7, where $v(P) = V(T,P)/V^{\ominus}(T^{\ominus})$ (equation 5 rearranged). This determined a range for K' (range 6.1 to 6.8, average at 6.5). Then, K_T was calculated with K' fixed at 6.5 and converted to equation form (see below). [f] From wave speed measurements on compacted, polycrystalline methane hydrate at 258.15 to 288.15 K and 27.6 to 62.1 MPa.[23] [g] $K_T = K_T^{\ominus} + k_1(T - 273.15) + k_2(T - 273.15)^2$. Note $k_2 = 0$ for H_2O (s) and hydrate. [h] Note: the equation of state for CH_4 (g) and f_{CH_4} was calculated using the empirically derived equation of state in Sychev et al.,[8] which covers the range 90.7 to 1000 K and 0.1 to 100 MPa.

large cages per 46 H_2O molecules. The relationship between hydrate number and cage occupancies is

$$n = 46(2x_S + 6x_L)^{-1} \quad (11)$$

The presence, depending on the hydrate number, of a significant number of vacant small and large cages in the methane hydrate structure also contributes to the Gibbs free energy of reaction 1. The configurational entropy term (in J mol H_2O^{-1} K^{-1})

$$\Delta S_{conf} = -R[3(x_L \ln x_L + (1 - x_L) \ln(1 - x_L)) + x_S \ln x_S + (1 - x_S) \ln(1 - x_S)]/23 \quad (12)$$

represents the entropy arising from the number of ways that the methane molecules and vacant sites can be arranged in both the small and large cages for a given fractional occupancy of those cages.[25] If all cages are filled with methane molecules, then $\Delta S_{conf} = 0$.

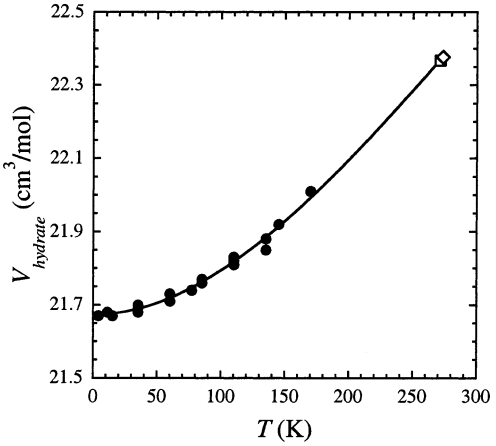

Figure 1. Measured methane hydrate molar volumes (filled circles) at 0.1 MPa and a range of temperatures (4−170 K).[15] The molar volume is further constrained at 271 K, 0.1 MPa by extrapolating the high-pressure unit-cell data of Klapproth et al.[16] to 0.1 MPa (open circle). The molar volume at standard state (diamond, Table 2) was calculated from a 3rd order polynomial fit to the data shown.

Finally, two additional factors have been considered. A term is added to eq 2 to account for the lowered activity of H_2O (l) due to the solution of methane in water. We calculated the concentration of dissolved methane gas using the Henry's law equation and constants cited in Sloan.[1] The Gibbs free energy of the reaction is made more positive by $-nRT \ln(1 - x_{CH_4(aq)})$, where n is the hydrate number in eq 1. This expression assumes that the activity coefficient for water is unity. A comparable correction is not needed for the H_2O (s) phase, for which the solubility of methane is negligible. We also considered the effect of the partial pressure of H_2O on the total pressure, which lowers the effective pressure of CH_4 (g). At low temperatures along the hydrate equilibrium boundary, the reaction pressures are low, the vapor pressure of H_2O is low, and the contribution of eq 8 to the Gibbs free energy of the reaction is relatively small. Although the vapor pressure of H_2O increases as T increases, the methane pressure increases much more rapidly, such that $P_{CH_4} \gg P_{H_2O}$. Thus, we did not include a correction for the negligible effect of the partial pressure of H_2O on the Gibbs free energy of the reaction (<1 J mol^{-1} $CH_4 \cdot nH_2O$ for all P and T conditions modeled).

The final equation for calculating the Gibbs free energy of reaction 1 is

$$\Delta G(T,P) = \Delta H^{\ominus}(T) - T\Delta S^{\ominus}(T) - T\Delta S_{conf} - nRT \ln(1 - x_{CH_4(aq)}) + \Delta \int_{P^{\ominus}}^{P} V(T,P)\, dP - RT \ln(f_P/f_{P^{\ominus}}) \quad (13)$$

As previously discussed, calculation of the Gibbs free energy

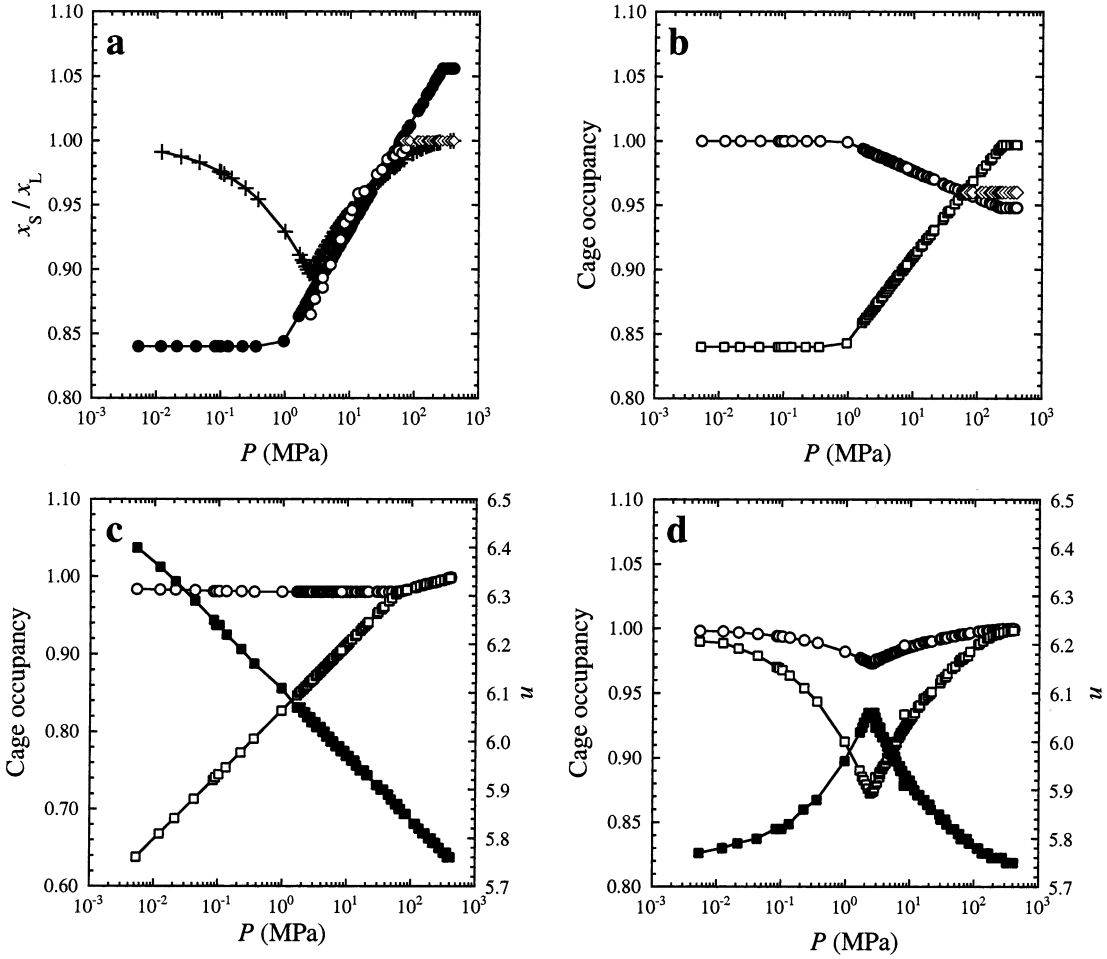

Figure 2. Methane distribution schemes between small and large cages in the hydrate structure. (a) Measured ratios of the fractional occupancy of methane in the small (x_S) and large cages (x_L) by Raman spectroscopy at pressures between 3.5 and 72.5 MPa[7] (open circles). Ratios for model B1 (filled circles) and B2 (open diamonds) and the ratios calculated using the program CSMHYD (plus signs) are also shown (see text). (b) Fractional cage occupancies in small (open squares) and large (open circles) cages for model B1, where $n = 5.99$. The further restriction that x_S/x_L remain ≤ 1 at higher pressures (model B2) is also shown (small and large cage occupancies equal-open diamonds). (c) Hydrate numbers (solid squares) and fractional cage occupancies in small (open squares) and large (open circles) cages for model C. (d) Hydrate numbers (solid squares) and fractional cage occupancies in small (open squares) and large (open circles) cages calculated using CSMHYD. The cage occupancy ratio is shown in (a).

of reaction 1 requires a few assumptions. The following sequence of steps was used: (1) The hydrate number and the distribution of methane between small and large cages was fixed, using models based on other sources of information and various assumptions (detailed below). (2) A third-law entropy for methane hydrate, $S^{\ominus}(T^{\ominus})$, was selected. (3) ΔG was calculated for 126 tabulated phase equilibria points between 0.0053 and 405 MPa.[1] The results were evaluated using

$$\chi^2 = \sum \frac{(\Delta G_{\text{hydrate}} - \Delta G_{\text{reactants}})^2}{\Delta G_{\text{reactants}}} \qquad (14)$$

which was summed for all P and T equilibrium pairs. This uses the sum of the reactants' contribution to ΔG for the expected value. Although ΔG was calculated for all 126 equilibrium pairs, we evaluated the quality of the fit using eq 14 for the 107 data pairs between 148.4 K and 0.0053 MPa and 304 K and 84 MPa, since the thermodynamic data for the reactants are well-established up to 100 MPa (Table 2, and there are no phase equilibria data points between 84 and 110 MPa). A "good" fit has a $\chi^2 \leq 107$ J mol^{-1}. Steps 2 and 3 were repeated until the minimum for eq 14 was found.

Ideally, the Gibbs free energy of reaction 1 should be zero at P and T conditions along the equilibrium boundary if the thermodynamic data are accurate. Given that the thermodynamic data for CH_4 and H_2O are relatively well-constrained, Gibbs free energy of reactions of ± 500 J mol^{-1} are considered acceptable. We ultimately assess the results by calculating the equilibrium temperature for a given equilibrium pressure along the phase boundary.

Results

Before modeling methane hydrate equilibria, we used the equations and thermodynamic data to calculate the P and T position of the ice (Ih) solid−liquid boundary for H_2O. The results are shown in Figure 3, and the agreement with the phase-equilibria data[26] is excellent over the range of the data (273.15−251.165 K and 0.1−210 MPa). The calculated T_{eq} at each P along the equilibrium boundary is within ± 0.4 K of the measured value.

Next we calculated the Gibbs free energy of reaction 1 for conditions ranging from 148.8 K, 0.0053 MPa to 320.0 K, 405 MPa (a total of 126 P, T pairs), which extends somewhat beyond the stated ranges of the various thermodynamic data (see Tables 1 and 2).

Model A: $n = 5.99$, $x_L = 0.98$. This model uses the directly measured hydrate number for methane hydrate.[4] The assumption

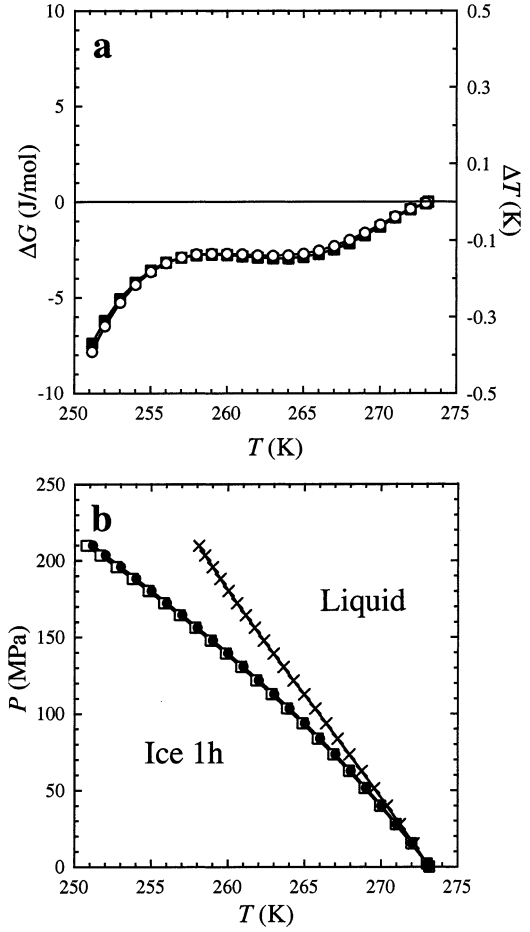

Figure 3. Results for calculating the reaction H_2O (s) = H_2O (l) using the thermodynamic data in Tables 1 and 2. (a) The calculated ΔG for measured equilibrium *P*, *T* pairs[26] (solid squares) and the difference between calculated and observed equilibrium temperatures for the reaction, using the measured P_{eq} and ΔG set to 0 J mol^{-1} (open circles), are shown. (b) Equilibrium *P*, *T* pairs for the reaction are plotted. The calculated equilibrium conditions (open squares) is in close agreement with the measured ones (solid circles). We also calculated the equilibrium conditions using the Clapeyron equation (X's), $T = T_{ref}\exp[(P - P_{ref})\Delta V_{tr}/\Delta H_{tr}]$, where reference conditions are 273.15 K, 0.1 MPa, ΔV_{tr} = 1.63 J mol^{-1} MPa^{-1}, and ΔH_{tr} = 6009 J mol^{-1}. This illustrates the poorer results obtained when the effects of large changes in *P* and *T* on the enthalpy and volume changes of the phase transition are not taken into account.

of approximately full large cages has been calculated previously using the statistical thermodynamic model.[24,27] This fixes the small cage occupancy at 0.90, the ratio of small to large cages at 0.918, and ΔS_{conf} at 1.342 J mol^{-1} K^{-1} for 1/*n* CH_4·H_2O. First, we calculated ΔG after selecting a value for $S^{\ominus}_{hydrate}(T^{\ominus})$ that minimizes χ^2 and assuming *n* is constant at 5.99. ΔG remains within 500 J mol^{-1} for most *P* and *T* pairs and shows some systematic variation with *T* (and *P*; Figure 4a). Second, we considered the effects of changing the hydrate number (to 5.92 or 6.06, the measured compositional uncertainty for methane hydrate annealed at 2 to 10 MPa along the equilibrium boundary).[4] ΔG is relatively unaffected at moderate *P* and *T* conditions (changing by <100 J mol^{-1} at 178 to 304 K and 0.04 to 85 MPa) but increasingly so at the extremes of low *T* or high *P* (Figure 4a). Third, we changed the distribution of hydrate between large and small cages by changing x_L to 0.95 or 1.00 while keeping the hydrate number constant (at $n = 5.99$). This had almost no effect on the modeling results (Table 3),

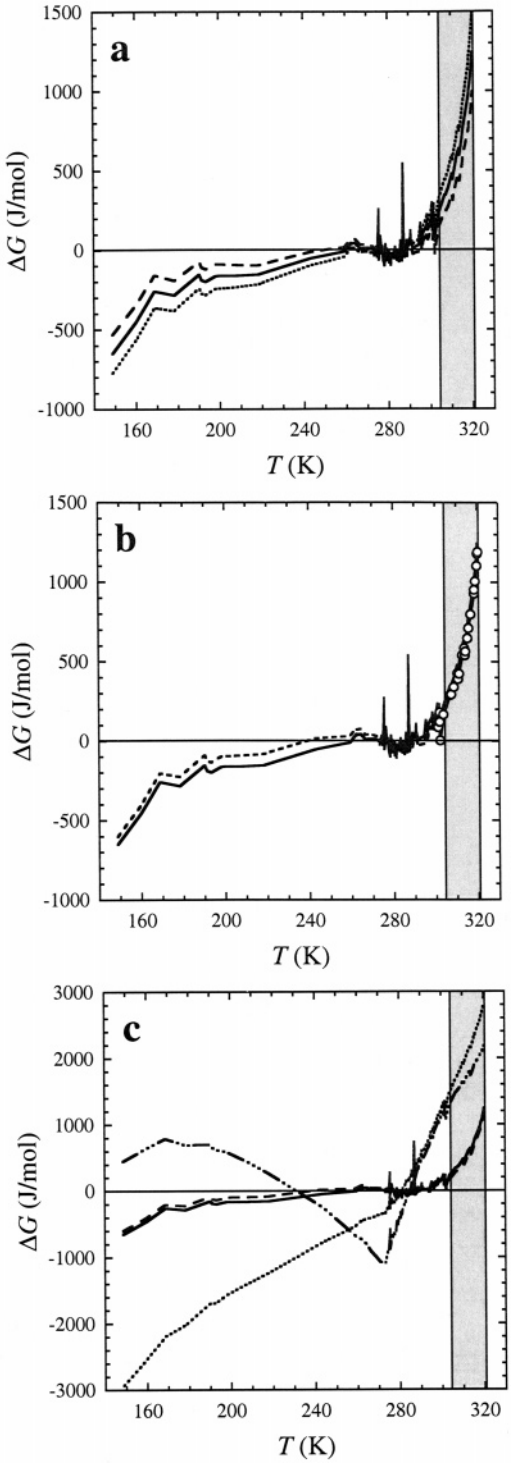

Figure 4. Results for calculating ΔG for reaction 1, using measured phase equilibria *P*, *T* pairs. The shaded areas highlight equilibrium conditions that were not included in the regression to find the minimum χ^2 and to fit $S^{\ominus}(T^{\ominus})$. Note that the spikes in ΔG correspond to *P*, *T* equilibrium pairs that deviate significantly from the trend established by the other data pairs. (a) Comparison of results for model A, showing the effect of changing the hydrate number and while x_L is fixed at 0.98: $n = 5.99$-solid line, $n = 5.92$-dashed line, $n = 6.06$-dotted line. (b) Results for models B1 (dashed line) and B2 (open circles, see text for model details), with results for model A ($n = 5.99$, $x_L = 0.98$; solid line) shown for comparison. (c) Comparison of results obtained using model C (dotted line) and model D (dashed-dotted line; hydrate number and cage occupancy distribution from the CSMHYD model). Results for models A (solid line) and B2 (dashed line)are plotted for comparison, and note the scale change from figures (a) and (b).

TABLE 3: Model A Parameters: Hydrate Number, Cage Occupancy, $S^{\ominus}(T^{\ominus})$ for Methane Hydrate (in J mol^{-1} K^{-1}), and χ^2 (in J mol^{-1})

	model A	vary n		vary x_L	
n	5.99	5.92	6.06	5.99	5.99
x_L	0.98	0.98	0.98	0.95	1.00
x_S/x_L	0.918	0.964	0.873	1.042	0.840
$S^{\ominus}(T^{\ominus})$	56.23	56.57	55.91	56.22	56.29
χ^2	18.2	11.3	28.2	18.2	18.2

TABLE 4: Parameters for Models B, C, and CSMHYD: Hydrate Number, Cage Occupancy, $S^{\ominus}(T^{\ominus})$ for Methane Hydrate (in J mol^{-1} K^{-1}), and χ^2 (in J mol^{-1})

	model A	model B1	model B2	model C	CSMHYD
n	5.99	5.99		varies	varies[a]
x_S/x_L	0.98	eq 10	modified	modified	varies[a]
$S^{\ominus}(T^{\ominus})$	56.23	56.24	56.24	56.15	56.52
χ^2	18.2	13.8	13.8	679.9	377.3

[a] Values calculated in program (see text, Figure 2d).

the results for ΔG are shifted <10 J mol^{-1} from the results for $x_L = 0.98$.

Several important observations can be made from model A. (1) The agreement between the phase equilibria and thermodynamic data is quite good overall ($\chi^2 \ll 107$ J mol^{-1}, Table 3). (2) At the thermal extremes, the deviation of ΔG from the zero point systematically becomes more negative (at low T) or positive (at high P). (3) The value for $S^{\ominus}(T^{\ominus})$ of $1/n$ $CH_4 \cdot H_2O$ is surprisingly robust, varying little from a value near 56.2 J mol^{-1} K^{-1}. This value lies between the standard-state entropies of solid and liquid H_2O (see Table 1). The presence of enclathrated methane molecules, which have rotational freedom within the cavities,[1] would be expected to contribute positively to the entropy of hydrate over that of ice. (4) Last, changing the fixed distribution of methane between the large and small cages has almost no effect on ΔG if the hydrate number remains constant. This does not mean that the contribution of the configurational entropy is not important, and we next consider what happens if the methane distribution between cages varies.

Model B: $n = 5.99$ and Use eq 10 to Calculate x_S/x_L. As previously discussed, Raman spectroscopic results[7] have indicated that, at least over the P range 3.5−72.5 MPa, the distribution of methane between small and large cages varies in a continuous manner, as shown in Figure 2a. We have applied this relationship to the entire data range, with the following imposed limitations. At pressures below 0.95 MPa, the ratio is fixed at 0.840 even though eq 10 predicts a continued decrease in the ratio. This marks the point where x_L becomes 1.00 (Figure 2b), as imposed by the fixed hydrate number of 5.99. Similarly, at pressures above 242 MPa, we have fixed the ratio at 1.056, the point at which x_S becomes 1.00 (model B1). Conversely, we could impose an upper limit on x_S/x_L of 1.00, such that $x_S \leq x_L$. This ratio is reached at 59 MPa using eq 10 (model B2, see Figure 2b). Allowing the distribution of methane between small and large cages to vary with pressure improved the fit over that of model A ($n = 5.99$, $x_L = 0.98$), while the value for $S^{\ominus}(T^{\ominus})$ remains essentially unchanged (Table 4, Figure 4b).

Model C: Allow n to Vary and Use eq 10 to Calculate x_S/x_L. Raman spectroscopic data, represented by eq 10, show an increase in the ratio x_S/x_L with increasing pressure. In the previous model, this meant that x_S increases as x_L decreases, because n is fixed. Alternatively, if the filling of one of the cages is relatively constant, for example x_L, then the trend represented by eq 10 leads to the constraint that n decreases with increasing pressure. This trend has been confirmed by direct measurement for other structure I hydrates ($CHClF_2$, CH_3Br, CH_3Cl, Cl_2, Xe, SO_2, and H_2S) at relatively low equilibrium pressures below 0.5 MPa.[28] We have devised a methane distribution where n decreases logarithmically with increasing pressure from 6.4 to 5.76 (Figure 2c), x_L remains relatively constant (between 0.980 and 0.998), and x_S increases from 0.638 to 0.998, with x_S/x_L determined by eq 10 then held constant at high pressure (as in model 2B, see above).

Model C yields the poorest result of all, both at low and high temperatures (Figure 4c, Table 4). The discrepancy between the model and the phase-equilibria data cannot be attributed to the uncertainties in the $S^{\ominus}(T^{\ominus})$, nor can it be tied to the specific methane distribution model used, as the differences in $-T\Delta S_{conf}$ are 2 orders of magnitude smaller than the observed discrepancies in ΔG. Instead, the difficulty arises in allowing n to vary so widely. Since we chose a somewhat arbitrary though reasonable range for n, we considered yet one other source of information to constrain the amount and distribution of methane, as described in model D.

Model D: n, x_S, and x_L from a Statistical Thermodynamics Model. In particular, we used the CSMHYD model developed by Sloan and co-workers[1] combined with the temperatures from the measured phase equilibria of methane hydrate as input, to obtain the following information for the system CH_4-H_2O: n, x_S, x_L, and P_{eq}. The values for the first three parameters are plotted in Figure 2d, and the calculated x_S/x_L is plotted in Figure 2a. We then took these parameters, and used them in our thermodynamic model, with results summarized in Table 4 and Figure 4c. Again, the results obtained by allowing n to vary are significantly poorer than in models A or B, where n is held constant. The calculated x_S/x_L agrees well with the Raman spectroscopy results over the measured pressure range (Figure 2a). However, the calculated maximum in hydrate number (Figure 2d), corresponding to minimums in x_S, x_L, and x_S/x_L, was not anticipated. The inflection point occurs at the P and T conditions of the quadruple point, where CH_4 (g), H_2O (l), H_2O (s), and $CH_4 \cdot nH_2O$ coexist.

Discussion

To summarize, using published thermodynamic data for the system CH_4-H_2O, we have calculated the ΔG for the formation of methane hydrate and obtained an estimate of the standard-state entropy of methane hydrate ($S^{\ominus}(T^{\ominus}) = 56.2$ J mol^{-1} K^{-1} for $1/n$ $CH_4 \cdot H_2O$). The calculations require extrapolation of the heat capacity and thermal expansion data for methane hydrate, as well as some assumptions for the distribution of methane between small and large cages in the hydrate structure. The "best" fit is obtained with Model B2, in which n is held constant at 5.99 and x_S/x_L is allowed to vary along the equilibrium boundary, yielding a ΔG within ± 200 J mol^{-1} of zero along the equilibrium boundary between 190 and 304 K and 0.08 and 84 MPa. ΔG increases at conditions outside this P, T range, but still remains within ± 500 J mol^{-1} up to pressures of 166 MPa. Other models (A, B1), in which n is held constant but the distribution of methane in small and large cages is different, also work well (Figure 4, Tables 3 and 4). However, when n is allowed to vary over a wide range (6.40 to 5.75, Model C; 6.1 to 5.75, CSMHYD model), the calculated ΔG varies significantly ($> \pm 1000$ J mol^{-1}) from the expected zero point for much of the equilibrium data (Figure 4c).

These variances in ΔG are equivalent to shifting the position of the methane hydrate equilibrium boundary in P and T space. Using P_{eq} and $\Delta G = 0$ J mol^{-1}, we calculated the T_{eq} conditions

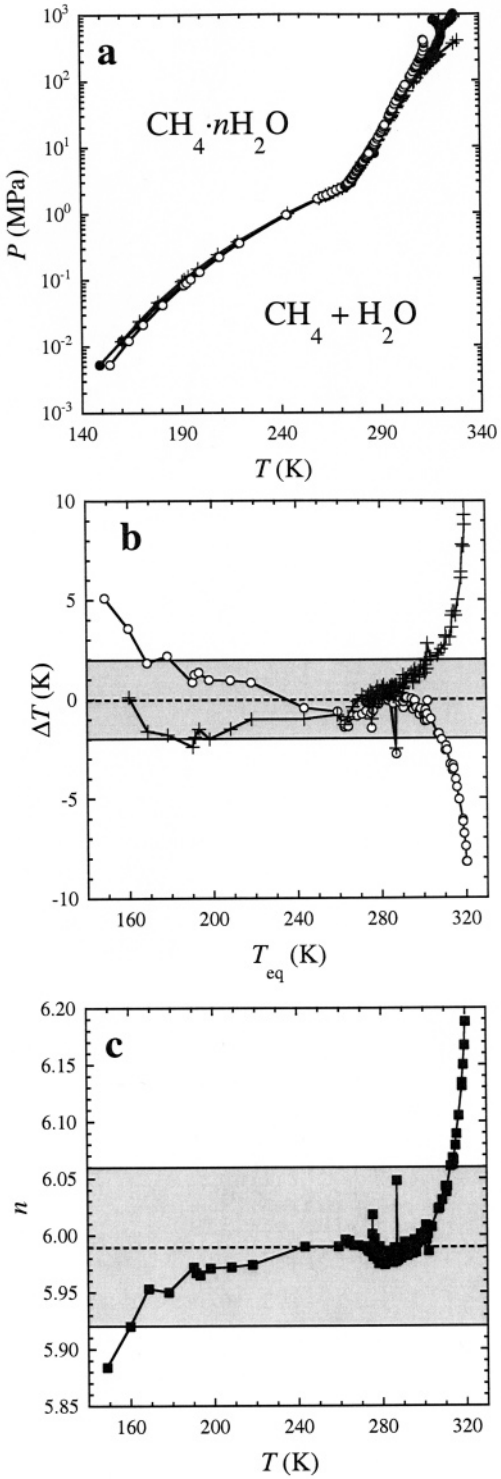

Figure 5. (a) Comparison of calculated equilibrium *P*, *T* pairs using a classical thermodynamic model (this study, model B2, open circles) and a statistical thermodynamic model (CSMHYD,[1] plus signs) to the published phase-equilibria data[1] (solid circles). (b) Temperature difference between the calculated and observed equilibrium temperatures for the classical thermodynamic model (open circles) and the statistical thermodynamic model (plus signs). Shaded area indicates a temperature difference of ±2 K. (c) Calculated hydrate number that shifts ΔG to 0 J mol^{-1} for model B2 (i.e., relax the fixed hydrate number constraint such that ΔG goes to zero). Shaded area indicates the hydrate number range of 5.99 + 0.07 measured by Circone et al.[4]

of equilibrium and compared these results to the observed phase-equilibria data and to the results from the statistical thermodynamic program CSMHYD (Figure 5a). Both the classical and statistical thermodynamic models do an excellent job of reproducing the phase equilibria curves of reaction 1 within 2 K of T_{eq} over the moderate *P* and *T* range stated above (Figure 5b). In fact, for the classical model, the deviation is within ±1 K between 266 and 302 K, a temperature range applicable to methane hydrate occurring in a geologic setting. At higher temperatures, the increasing uncertainties arising from the larger extrapolations of the thermodynamic data (hydrate heat capacity, hydrate equation of state, methane gas fugacity, and/or the concentration of dissolved methane in water) likely contribute to the observed deviation; however, we are unable to isolate which extrapolation(s) are primarily responsible for the discrepancy. At low temperature, extrapolations are unnecessary, and other possibilities must be considered. An obvious choice is to relax the constraint that *n* is constant. Using model B2, and allowing *n* to vary such that $\Delta G = 0$, we found that *n* remains within the directly measured range of 5.99 ± 0.07 for most of the *P* and *T* pairs (Figure 5c). This modest variation in *n* is much less than the range assumed in model C or that shown in Figure 2d for the CSMHYD results. In fact, the calculated hydrate compositions from the CSMHYD model cannot be reconciled with the thermodynamic calculations in this study, which are governed by the experimentally determined properties of methane hydrate.

Conclusions

A classical thermodynamic model, using experimentally determined data for phases in the system CH_4-H_2O, has been successfully developed and used to calculate the phase equilibria of methane hydrate over a wide range of geologically relevant *P* and *T* conditions. This model has two main strengths: (1) it uses directly measurable parameters to calculate equilibrium conditions for the methane hydrate formation reaction, and (2) the equations can be used to calculate the Gibbs free energy of methane hydrate at conditions other than equilibrium. While the thermodynamic data calculations in this study have yielded a robust estimate, low temperature heat capacity measurements are needed to determine the third-law entropy of methane hydrate directly. Further constraints on the high-temperature thermal expansion of methane hydrate are also needed. Certainly, the main question that remains is whether the hydrate number varies with the *P* and *T* conditions and, if so, how widely does it range. While both NMR and Raman spectroscopy techniques indicate that the distribution of methane between small and large cages in the hydrate structure does indeed vary, these results do not constrain the actual hydrate number. The results from the classical thermodynamic model are wholly consistent with little or no variation in hydrate number over a wide range of *P* and *T* conditions and are in agreement with the directly measured compositions between 2 and 10 MPa. Ultimately, this issue can only be resolved through direct measurement.

Acknowledgment. We thank William B. Durham, William F. Waite, and two anonymous reviewers for providing helpful reviews of this manuscript. We acknowledge the financial support of the USGS Gas Hydrate Project and the DOE Methane Hydrate Research and Development Program.

References and Notes

(1) Sloan, E. D. *Clathrate Hydrates of Natural Gases*, 2nd ed; Marcel Dekker: New York, 1998.

(2) van der Waals, J. H.; Platteuw, J. C. In *Advances in Chemical Physics vol. II*; Prigogine, I., Ed.; Interscience Publishers: New York, 1959; p 1.

(3) Fei, Y.; Saxena, S. K. *Phys. Chem. Minerals* **1986**, *13*, 311.
(4) Circone, S.; Kirby, S. H.; Stern, L. A. *J. Phys. Chem. B* **2005**, *109*, 9468.
(5) Galloway, T. J.; Ruska, W.; Chappelear, P. S.; Kobayashi, R. *Ind. Eng. Chem. Fundam.* **1970**, *9*, 237.
(6) Handa, Y. P. *J. Chem. Thermodyn.* **1986**, *18*, 915.
(7) Kini, R. A.; Huo, Z.; Jager, M. D.; Bollavaram, P. In *Proc. Fourth Internatl. Conf. Gas Hydrates*, Yokohama, Japan, 2002, 867.
(8) Sychev, V. V.; Vasserman, A. A.; Zagoruchenko, V. A.; Kozlov, A. D.; Spiridonov, G. A.; Tsymarny, V. A. *Thermodynamic Properties of Methane*; Hemisphere Publishing Corporation: Washington, 1987.
(9) Robie, R. A.; Hemingway, B. S.; Fisher, J. R. U. S. Geological Survey Bulletin 1452; 1979.
(10) *CODATA Key Values for Thermodynamics*; Cox, J. D., Wagnan, D. D., Medvedev, V. A., Eds.; Hemisphere Publishing Corporation: New York, 1989.
(11) Ginnings, D. C.; Corruccini, R. J. *J. Res., Natl. Bur. Stds.* **1947**, *38*, 583.
(12) Röttger, K.; Endriss, A.; Ihringer, J.; Doyle, S.; Kuhs, W. F. *Acta Crystallogr.* **1994**, *B50*, 644.
(13) Dorsey, N. E. *Properties of Ordinary Water-Substance*; Reinhold Publishing Corporation: New York, 1940.
(14) *CRC Handbook of Chemistry and Physics*; Weast, R. C., Ed.; CRC Press: Boca Raton, FL, 1985.
(15) Rawn, C. J.; Chakoumakos, B. C.; Rondinone, A. J.; Stern, L. A.; Circone, S.; Kirby, S. H.; Ishii, Y.; Jones, C. Y.; Toby, B. H.; Sassen, R. Neutron and X-ray powder diffraction characterization of a variety of structure I and structure II clathrate hydrates, in preparation.
(16) Klapproth, A.; Goreshnik, E.; Staykova, D.; Klein, H.; Kuhs, W. F. *Can. J. Phys.* **2003**, *81*, 503.
(17) Gagnon, R. E.; Kiefte, H.; Clouter, M. J.; Whalley, E. *J. Physique* **1987**, *48*, C1−23.
(18) Gammon, P. H.; Kiefte, H.; Clouter, M. J.; Denner, W. W. *J. Glaciol.* **1983**, *29*, 433.
(19) Gagnon, R. E.; Kiefte, H.; Clouter, M. J.; Whalley, E. *J. Chem. Phys.* **1990**, *92*, 1914.
(20) Proctor, T. M. *J. Acoustical Soc. Am.* **1966**, *39*, 972.
(21) Gagnon, R. E.; Kiefte, H.; Clouter, M. J. *J. Chem. Phys.* **1988**, *89*, 4522.
(22) Burnham, C. W.; Holloway, J. R.; Davis, N. F. *Thermodynamic properties of water to 1,000 °C and 10,000 bars*; Geological Society of America: Boulder, CO, 1969; Special Paper no. 132.
(23) Helgerud, M. B.; Waite, W. F.; Kirby, S. H.; Nur, A. *Proc. Fourth Internatl. Conf. Gas Hydrates*, Yokohama, Japan, 2002, p 711.
(24) Ripmeester, J. A.; Ratcliffe, C. I. *J. Phys. Chem.* **1988**, *92*, 337.
(25) Greenwood, N. N. *Ionic Crystals Lattice Defects and Nonstoichiometry*; Butterworth: London, 1968.
(26) Wagner, W.; Saul, A.; Pruss, A. *J. Phys. Chem. Ref. Data* **1994**, *23*, 516.
(27) Huo, A.; Hester, K.; Sloan, E. D. *AIChE J.* **2003**, *49*, 1300.
(28) Cady, G. H. *J. Phys. Chem.* **1983**, *87*, 4437.